Acta Pharmaceutica Sinica B 2022;12(5):2315–2329

Chinese Pharmaceutical Association
Institute of Materia Medica, Chinese Academy of Medical Sciences

Acta Pharmaceutica Sinica B

www.elsevier.com/locate/apsb
www.sciencedirect.com

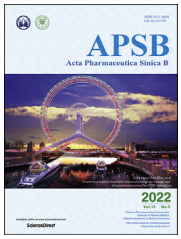

ORIGINAL ARTICLE

The substitution of SERCA2 redox cysteine 674 promotes pulmonary vascular remodeling by activating IRE1α/XBP1s pathway

Weimin Yu[a,b], Gang Xu[c,d], Hui Chen[a], Li Xiao[a], Gang Liu[a,e], Pingping Hu[a], Siqi Li[a], Vivi Kasim[f], Chunyu Zeng[g], Xiaoyong Tong[a,*]

[a]*School of Pharmaceutical Sciences, Chongqing University, Chongqing 401331, China*
[b]*Institute of Health Biological Chemical Medication, Chongqing Institute of Green and Intelligent Technology, Chinese Academy of Sciences, Chongqing 400714, China*
[c]*Institute of Medicine and Equipment for High Altitude Region, College of High Altitude Military Medicine, Army Medical University (Third Military Medical University), Chongqing 400038, China*
[d]*Key Laboratory of High Altitude Medicine, People's Liberation Army, Chongqing 400038, China*
[e]*Henan Key Laboratory of Medical Tissue Regeneration, College of Basic Medical Sciences, Xinxiang Medical University, Xinxiang 453003, China*
[f]*Key Laboratory of Biorheological Science and Technology, Ministry of Education, College of Bioengineering, Chongqing University, Chongqing 400044, China*
[g]*Department of Cardiology, Daping Hospital, Army Medical University (Third Military Medical University), Chongqing 400042, China*

Received 1 September 2021; received in revised form 14 December 2021; accepted 29 December 2021

KEY WORDS

Pulmonary hypertension;
Sarcoplasmic/endoplasmic reticulum Ca^{2+} ATPase;
Pulmonary vascular remodeling;
Pulmonary artery smooth muscle cell;
Endoplasmic reticulum stress;
Oxidative stress

Abstract Pulmonary hypertension (PH) is a life-threatening disease characterized by pulmonary vascular remodeling, in which hyperproliferation of pulmonary artery smooth muscle cells (PASMCs) plays an important role. The cysteine 674 (C674) in the sarcoplasmic/endoplasmic reticulum Ca^{2+} ATPase 2 (SERCA2) is the critical redox regulatory cysteine to regulate SERCA2 activity. Heterozygous *SERCA2* C674S knock-in mice (SKI), where one copy of C674 was substituted by serine to represent partial C674 oxidative inactivation, developed significant pulmonary vascular remodeling resembling human PH, and their right ventricular systolic pressure modestly increased with age. In PASMCs, substitution of C674 activated inositol requiring enzyme 1 alpha (IRE1α) and spliced X-box binding protein 1 (XBP1s) pathway, accelerated cell cycle and cell proliferation, which reversed by IRE1α/XBP1s pathway inhibitor 4μ8C. In addition, suppressing the IRE1α/XBP1s pathway prevented pulmonary vascular

*Corresponding author.
E-mail address: xiaoyongtong@cqu.edu.cn (Xiaoyong Tong).

Peer review under responsibility of Chinese Pharmaceutical Association and Institute of Materia Medica, Chinese Academy of Medical Sciences.

https://doi.org/10.1016/j.apsb.2021.12.025

remodeling caused by substitution of C674. Similar to SERCA2a, SERCA2b is also important to restrict the proliferation of PASMCs. Our study articulates the causal effect of C674 oxidative inactivation on the development of pulmonary vascular remodeling and PH, emphasizing the importance of C674 in restricting PASMC proliferation to maintain pulmonary vascular homeostasis. Moreover, the IRE1α/XBP1s pathway and SERCA2 might be potential targets for PH therapy.

1. Introduction

Pulmonary hypertension (PH) is a life-threatening disease with a mean pulmonary arterial pressure (PAP) $\geq$ 25 mmHg at rest. PH is clinically divided into five groups. Group 1 is pulmonary artery hypertension (PAH), and others are all associated with various diseases[1−3]. PAH is a particularly severe and progressive form with slow clinical onset and progressive deterioration, characterized by plexiform lesions[2,4,5]. Pulmonary vascular remodeling is the main cause of PH. Due to the limited lung samples of PH patients and the lack of appropriate animal models to simulate human PH, the pathogenesis of PH remains controversial[5,6].

Sarcoplasmic/endoplasmic reticulum Ca^{2+} ATPase (SERCA) is key to maintaining Ca^{2+} homeostasis by transporting Ca^{2+} from cytoplasm to sarcoplasmic reticulum (SR) and endoplasmic reticulum (ER), to maintain low Ca^{2+} concentration in the cytoplasm and high Ca^{2+} concentration in SR/ER. SERCA2 (gene *Atp2a2* in mouse and *ATP2A2* in human) is the main subtype of vascular SERCA, mainly including *Atp2a2a* and *Atp2a2b* genotypes, in which *Atp2a2b* is a housekeeping gene. The *S*-glutathiolation of cysteine 674 (C674) regulates the activity of SERCA2 under physiological conditions, but this modification is prevented by its irreversible oxidation in pathological situations with increased reactive oxygen species (ROS)[7]. Increased intracellular Ca^{2+} level is a well-known contributor to the proliferation of smooth muscle cells (SMCs). Inhibition of SERCA2 activity induces hypoxic pulmonary vein remodeling[8]. The decrease of SERCA2a is involved in monocrotaline-induced rat pulmonary artery (PA) remodeling[9]. The roles of C674 and its oxidative inactivation and SERCA2b in pulmonary vascular remodeling remain unclear. Here, we used heterozygous *SERCA2* C674S knock-in mice (SKI), where one copy of C674 was substituted by serine (S674), to indicate partial C674 oxidative inactivation[10]. The results showed that SKI developed significant pulmonary vascular remodeling resembling human PH, and their right ventricular systolic pressure (RVSP) modestly increased with age. In pulmonary artery smooth muscle cells (PASMCs), the substitution of C674 by S674 accelerated cell cycle and promoted cell proliferation by activation of inositol requiring enzyme 1 alpha (IRE1α) and spliced X-box binding protein 1 (XBP1s) pathway. Similar to SERCA2a[9], SERCA2b is also important to contain the proliferation of PASMCs. This study provides a novel mechanism of SERCA2 dysfunction in promoting PASMC proliferation that is by the activation of the IRE1α/XBP1s pathway and confirming for the first time that suppressing IRE1α/XBP1s pathway prevents pulmonary vascular remodeling.

2. Material and methods

2.1. Animals

The Ethics Committee of Chongqing University Three Gorges Hospital (Chongqing, China) approved all animal care and study protocols that were complied with the guidelines of the ethical use of animals. Animal experiments had been performed according to the ARRIVE guidelines and EU Directive 2010/63/EU for the use and care of animals. We made all efforts to minimize animal suffering and reduce the number of animals used. We bred and housed mice in the laboratory animal room at Chongqing University (Chongqing, China) under specific pathogen-free conditions. Mice lived in open polypropylene cages with clean chip bedding, and the animal rooms were maintained at a controlled temperature (22 $\pm$ 3 °C) with a 12-h-cycle of light and dark. Five mice in each cage were free to drink water and regular diet. To obtain tissues, all mice were killed by intraperitoneal injection once with avertin (2,2,2-tribromoethanol; Cat# T48402; Sigma−Aldrich, Darmstadt, Germany) at a dose of 250 mg/kg body weight as we previously described[11]. We chose avertin instead of isoflurane or ketamine combination because it does not need to consider the anesthetic effect and is suitable for the final execution of animals.

2.2. SERCA2 C674S knock-in mouse construct

All mice used in this study were C57BL/6J background (the Jackson Laboratory, Bar Harbor, ME, USA). The construct of SKI was generated as previously described[10]. Briefly, the genetic variation is TGT at site 674 (cysteine, C674) to TCC (serine, S674) in exon 14 of SERCA2 governed by the unaltered upstream native *SERCA2* promoter. Sequencing of both genomic DNA and cDNA from heart verified the presence of the C674S mutation. Homozygous SKI mice died before birth, so only heterozygous SKI mice that express 50% of C674 and 50% of S674 were used in this study, and their littermate wild-type mice (WT) without S674 were used as controls. From our preliminary data, SKI male and female mice showed the same trend in pulmonary vascular remodeling, and it seemed that male mice have relatively more severe lesions than female mice of the same age. In order to avoid the influence of gender on different age groups, all experiments used healthy male mice, whose number in each study is indicated in the corresponding figure legend.

2.3. Hypobaric hypoxia-induced PH

Male C57/BL6J mice (18−22 g) at 2 months old were randomly divided into two groups, normoxia and hypoxia. Hypoxic mice

exposed to a hypobaric chamber (depressurized to 360 mmHg equivalent to 10% O_2) at simulated altitude of 5800 m, the same condition as common practices in literature for achieving hypoxia[12]. Normoxic mice (21% O_2) maintained at 308 m altitude of Chongqing. Twenty-eight days later, took lungs for immunochemistry (middle lobes of right lung) and protein analysis (other parts of lung). The hypobaric chamber was maintained at simulated altitude of 5000 m when replacing food, water, and clean chip bedding or collecting lungs. An altitude of 5000 m is safe for human beings to carry on these activities, but it cannot be higher.

2.4. *In vivo treatment*

The 4-week-old male WT and SKI were randomly divided into two groups and given the specific inhibitor of IRE1α endoribonuclease activity, 4μ8C[13] (10 mg/kg/day; MCE, Shanghai, China), or its solvent control individually for 4 weeks *via* intraperitoneal injection once a day. 4μ8C dissolved in solvent containing 5% DMSO, 40% PEG400, 10% Tween 80, and 45% saline.

2.5. *Measurement of right ventricular parameters*

In order to obtain a more stable anesthetic effect, we used urethane instead of isoflurane or ketamine combinations. Mice were anesthetized once with 15% urethane (Chengdu Huaxia Chemical Reagent Co., Ltd., China) at a dose of 10 mL/kg body weight. One end of a polyethylene catheter is inserted into the right ventricle *via* right external jugular vein, and the other end of the catheter connected to a transducer. The right ventricular parameters, including right ventricular systolic pressure (RVSP) and right ventricle end-diastolic pressure (RVEDP), were simultaneously recorded by a physiological recorder (PowerLab system, AD Instruments, Castle Hill, NSW, Australia), and analyzed by the chart program supplied by the system. After all measurements were complete, the right ventricle (RV) free wall, interventricular septum (S), and the left ventricle (LV) were removed to measure their weight. The Fulton index [RV/(LV + S) weight] was used to assess right ventricular hypertrophy.

2.6. *Histology, immunohistochemistry, and immunofluorescence in lung sections*

The middle lobes of right lung were fixed in 4% paraformaldehyde for 24 h, and then in 30% sucrose solution for 24 h. After that, lungs were embedded in optimum cutting temperature compound (the middle biggest lobe) or paraffin (the middle second biggest lobe) to prepare serial sections at a thickness of 7 μm. The leftover lungs were snap-frozen in liquid nitrogen and stored at −80 °C for protein analysis. Serial sections of lung for each mouse were prepared and stained individually with Verhoeff-Van Gieson (VVG) and Masson's trichrome for morphological analysis. Masson's trichrome staining showed that the fibrosis was blue. For SERCA2 C674-SO_3H immunohistochemistry staining, lung sections were heated in 10 mmol/L citrate acid buffer for antigen recovery. Blocked in goat serum, sections were incubated with primary polyclonal antibodies against SERCA2 C674-SO_3H (Cat# A300-BL2103; Bethyl Laboratories, Inc., Montgomery, TX, USA) overnight at 4 °C according to the staining procedure of HRP-DAB kit (Cat# CW0125M; CWBIO, Beijing, China). For immunofluorescence analysis of lung cryosections, incubated sections at 4 °C for 12 h with specific antibodies against the following proteins: α-smooth muscle actin (α-SMA; Cat# MA5-11547; Invitrogen, Carlsbad, CA, USA), von Willebrand factor (vWF; Cat# 11778-1-A; Proteintech, Wuhan, China), Ki67 (Cat# ab15580; abcam, Cambridge, UK), cyclin A1 (Cat# AP51052; abcepta, Suzhou, China), cyclin A2 (Cat# 18202-1-AP, Proteintech), cyclin B1 (Cat# 55004-1-AP, Proteintech), and XBP1s (Cat# 24868-1-AP, Proteintech), followed by Alexa Fluor 488 goat anti-rabbit IgG (H + L) (Cat# 111-545-144; Jackson Immunoresearch, West Grove, PA, USA) or Cy3-conjugated Affinipure goat anti-mouse IgG (H + L) (Cat# SA00009-1, Proteintech) for 2 h. 4′,6-Diamidino-2-phenylindole (DAPI; Cat# C0065; Solarbio, Beijing, China) stained nuclei for 10 min. Fluorescence images were taken by the microscope (Leica DM6, Germany) and analyzed by Las X software (Leica). Four individual observers blinded to the experimental groups quantified the staining of SERCA2 C674-SO_3H and XBP1s. The positive areas (brown for SERCA2 C674-SO_3H staining, green for XBP1s staining) were scored according to the scoring standard of 0−4, in which 0 is negative intensity, 1 is weak intensity, 2 and 3 are medium intensity and 4 is strong intensity. In the distal pulmonary arterioles (< 50-μm-diameter), the levels of muscularization were evaluated by α-SMA and vWF co-staining. vWF staining showed the endothelial cells (ECs) of arterioles, and α-SMA staining showed the existence of SMCs outside the endothelial layer. Full muscularization showed that α-SMA staining formed a complete circle, non-muscularization showed no α-SMA staining, and partial muscularization was between them. The total number of arterioles was counted to calculate their relative percentages. In PA tunica media indicated by α-SMA staining, the percentage of Ki67-positive proliferating cells in the total number of nuclei shown by DAPI staining was calculated. The calculation results by different observers in at least three random fields were comparable, and data were represented by the average value from different observers.

2.7. *Morphology analysis of pulmonary vascular lesions*

Tunica media thickness was used to evaluate tunica media hypertrophy in PAs (outer diameter of 50−100 μm) identified by α-SMA staining, which was calculated as [(outer diameter−inner diameter)/outer diameter] × 100%. Cellular neointima derived from ECs in small PAs (around 50 μm diameter) is characterized by remarkable cellular filling inside of lumen identified by vWF staining, whose incidence was calculated by the ratio of the number of PAs with cellular neointima to the total number of PAs. VVG staining confirmed pulmonary artery thrombosis, whose incidence was calculated by the number of mice with thrombus in the total number of mice. Evaluated the severity of concentric or eccentric neointimal lesions derived from SMCs in PAs according to the ratio of neointimal area to lumen area: score 0, ratio = 0; score 1, 0 < ratio < 0.25; score 2, 0.25 ≤ ratio < 0.50; score 3, 0.50 ≤ ratio < 0.75; score 4, ratio > 0.75. Aneurysm-like plexiform lesions were characterized by distinguishing aneurysm-like structures derived from SMCs around the PAs. Evaluated their severity according to the ratio of aneurysm-like lesion area to lumen area: score 0, ratio = 0; score 1, 0 < ratio < 0.25; score 2, 0.25 ≤ ratio < 0.50; score 3, 0.50 ≤ ratio < 0.75; score 4, ratio > 0.75. Stalk-like plexiform lesions were characterized by disorganized stalk-like structures derived from ECs and SMCs inside of PA lumen. Evaluated the severity of stalk-like plexiform lesions according to the ratio of lesion area to lumen area: score 0, ratio = 0; score 1, 0 < ratio < 0.05; score 2, 0.05 ≤ ratio < 0.10; score 3, 0.10 ≤ ratio < 0.15; score 4, ratio > 0.15. We scored

overall PA lesions based on the standard of Heath-Edward classification that later revised by Wagenvoort et al.[14], in which the plexiform lesions were divided into four grades (I–IV). Heath-Edward score 0, normal PAs; score 1 (grade I), tunica media hypertrophy of PAs, muscularization of distal pulmonary arterioles, without intimal alteration; score 2 (grade II), tunica media hypertrophy, cellular neointima in the smaller PAs; score 3 (grade III), extensive vascular occlusion with intimal lamellar changes; score 4 (grade IV), plexiform lesions, thrombosis. Venous lesions were characterized by thickening of pulmonary veins and dense cell clusters derived from SMCs inside and outside pulmonary veins. The severity of venous lesions was evaluated according to the ratio of the venous wall area to lumen area: score 0, ratio $<$ 0.25 (its ratio in normal vein $<$ 0.25); score 1, 0.25 $<$ ratio $<$ 0.50; score 2, 0.50 $\leq$ ratio $<$ 0.75; score 3, 0.75 $\leq$ ratio $<$ 1.00; score 4, ratio $>$ 1.00. We then evaluated the neointimal lesions and plexiform lesions in PAs by VVG staining or α-SMA staining, and vein lesions by VVG staining.

2.8. Isolation and culture of PASMCs

PASMCs were isolated from 8-week-old male WT and SKI using an explant method. Briefly, rinsed the PA branches below grade 3 with sterile saline to remove excess blood, and digested with 0.2% collagenase II (Cat# LS004177; Worthington Biochemical, Lakewood, NJ, USA) for 5 min. Cut the artery longitudinally, and scraped intima and adventitia to remove ECs and fibroblasts. The left tissue adhered to the bottom of a 35 mm dish and was cultured in Dulbecco's modified Eagle's medium (DMEM) supplemented with 20% fetal bovine serum (FBS) (Cat# FSP500; ExCell Bio, Shanghai, China) and antibiotics (100 U/mL penicillin and 100 μg/mL streptomycin; Solarbio) at 37 °C in a humidified atmosphere containing 5% CO_2. Once the cells grew from the explants to a radius of around 0.5 cm, digested with 0.2% trypsin and cultured them in DMEM containing 10% FBS and antibiotics. α-SMA and SM22α (Cat#10493-1-AP; Proteintech) positive immunostaining confirmed PASMC phenotype, while its CD31 (Cat#14-0311-82; Invitrogen) staining was negative. We have tested up to 10 passages and found that WT and SKI PASMCs still showed phenotypes similar to those of the earlier passages. To avoid PASMCs losing their phenotype in higher passages, we used PASMCs from passages 3 to 8, so that we can obtain enough cells to test their mechanisms while still maintaining the PASMC phenotype.

2.9. Real-time quantitative PCR (qPCR)

Total RNA was isolated from PASMCs using TRIzol reagent (Cat#15596026, Invitrogen), and retro-transcribed to cDNA using cDNA PCR kit (Cat#RR037Q; Takara Bio Inc., Shiga, Japan). Real-time qPCR was performed using SYBR-Green-based detection (Cat# RR420L; Takara Bio Inc.) with primers commercially synthesized (Sangon Biotech, Shanghai, China). Mouse gene specific primer sequences were listed in Supporting Information Table S1. The following cycling conditions were used: denaturation, annealing, and extension at 95, 57, and 72 °C for 10, 30, and 10 s, respectively, for 40 cycles. β-Actin was used as control. The relative copy number of *Atp2a2* (SERCA2) was analyzed using a $2^{-\Delta Ct}$ method that corrected the expression level of *Atp2a2a* (SERCA2a) or *Atp2a2b* (SERCA2b) by β-actin, and then represented the data as a ratio to WT *Atp2a2a*. The relative expression of *Xbp1* mRNA was analyzed using the comparative Ct method ($2^{-\Delta\Delta Ct}$) that was the relative expression level of *Xbp1* in SKI to its expression level in WT after being corrected by β-actin individually.

2.10. Western blot

Lysed lungs or PASMCs in RIPA buffer (Cat# E1WP106; EnoGene, Nanjing, China), and separated proteins by SDS-PAGE electrophoresis using standard methods, then transferred to PVDF membrane. Immunoblotted PVDF membrane at 4 °C overnight with specific antibodies against the following proteins: SERCA2 (C498 antibody was a customized polyclonal antibody from Bethyl Laboratories, Inc.; 110 kDa), SERCA2 C674-SO_3H (Cat# A300-BL2103; Bethyl Laboratories, Inc.; 110 kDa), phosphorylated IRE1α (p-IRE1α; Cat# GTX132808; Genetex, TX, USA; 133 kDa), IRE1α (Cat# 3294; CST, Danvers, MA, USA; 130 kDa), binding immunoglobulin protein (BIP; Cat# E90019; EnoGene; 78 kDa), activating transcription factor 6 (ATF6; Cat# E90009A; EnoGene; 75 kDa), unspliced XBP1 (XBP1u; 25997-1-AP; Proteintech; 36 kDa), XBP1s (Cat# 658802; Biolegend, San Diego, CA, USA; 55 kDa), cyclin A1 (55 kDa), cyclin A2 (50 kDa), cyclin B1 (60 kDa), cyclin D1 (Cat# 60186-1-Ig; Proteintech; 34 kDa), cyclin dependent kinase 1 (CDK1; Cat# AP16160b; abcepta; 35 kDa), CDK2 (Cat# AP7518d; abcepta; 34 kDa), β-actin (Cat# E12-051-3; EnoGene; 42 kDa), followed by incubation with HRP-conjugated goat-anti-rabbit secondary antibody (Cat# SSA003; Sino Biological Inc., Beijing, China) 1 h at room temperature. Proteins were visualized with an X-Ray film system (Fujifilm, Japan) or ChemiDoc TM Touch System (Bio-Rad, USA). Band density was quantified by NIH Image J software and normalized to β-actin, and expressed as a ratio to WT or solvent (vector) control.

2.11. Intracellular calcium measurements

Seeded WT and SKI PASMCs on glass coverslips overnight in a 24-well plate. According to the manufacture's procedure, the cells were loaded with 4 μmol/L Fluo-4 AM (Cat# F8500; Solarbio) in HBSS (Cat#SH30030.02; Hyclone, Logan, UT, USA) containing 0.02% pluronic F12 in the dark at 37 °C for 20 min, then were retained for 40 min after adding 2-fold volume of HBSS containing 10% FBS. Washed cells 5 times with HEPES buffer, and incubated them in the dark at 37 °C for 10 min. Recorded the fluorescence signals with excitation Ex 494 nm and emission Em 516 nm by fluorescence microscopy (Leica DM6) and analyzed the average fluorescence signals by Las X software.

2.12. Cell proliferation assay

Cell proliferation rate was determined by counting the cell number or using a tetrazolium-based non-radioactive proliferation assay kit (Quick Cell Proliferation Assay Kit II; Cat# K301-500; Bio-Vision, San Francisco, CA, USA). For counting cell number, PASMCs were seeded in 12-well plate at a density of 5×10^4 cells per well in DMEM supplemented with 0.2% FBS for 24 h, and then switched to DMEM containing 10% FBS for 48 h. Harvested cells by mild trypsinization and counted them with a hemocytometer. For tetrazolium-based assay, PASMCs were seeded in 96-well plate at a density of 5×10^3 cells per well in DMEM supplemented with 0.2% FBS overnight. Cell proliferation was stimulated by medium supplemented with 10% FBS, and 0.2% FBS medium was used as a control. Culture medium was changed

with high or low serum daily. The cell number in each well was determined 72 h later by the proliferation assay kit according to the manufacturer's protocol.

2.13. 5-Ethynyl-2′-deoxyuridine (EdU) incorporation assay

EdU incorporation was performed using Cell Light EdU Apollo488 *In Vitro* Imaging Kit (Cat# C10310-3; RiboBio, Guangzhou, China) according to the manufacturer's instruction. Nuclei were stained with Hoechst 33258 (Cat# C0021; Solarbio). Monitored the fluorescence signals by microscopy (Leica DM6) and analyzed them by Las X software.

2.14. Flow cytometry analysis of cell cycle

PASMCs (2×10^5 cells) were cultured in 60 mm dish with 0.2% FBS DMEM for 24 h, and then switched to DMEM containing 10% FBS for 24 h. Harvested cells by mild trypsinization and centrifugation. Pre-chilled phosphate buffered solution (PBS) washed cells twice and then used pre-chilled 70% ethanol to fix cells at 4 °C overnight. The next day, cells were collected by centrifugation and washed with 1 mL of PBS, then added 500 μL PBS containing 50 μg/mL propidium iodine (PI), 100 μg/mL RNase A, 0.2% Triton X-100, incubating at 4 °C for 30 min in the dark. Cell cycle assay was determined by flow cytometry (CytoFLEX A00-1-1102; Beckman Coulter, Brea, CA, USA), and data were analyzed by using CytExpert software (Beckman Coulter). Used ModFit LT 3.2 software (Verity Software House, Topsham, ME, USA) to measure the percentage of cells in each phase of the cell cycle.

2.15. Cell treatments

For hypoxia study, WT PASMCs were cultured in either normoxic condition (21% O_2) or hypoxic condition (4% O_2) for 24 h in DMEM containing 0.2% FBS and antibiotics, then quickly collected in RIPA buffer in normoxic condition for Western blot. For *in vitro* treatments of 4μ8C or inhibitor of ER stress, 4-phenylbutyric acid (4-PBA, MCE), cultured SKI PASMCs in 0.2% FBS DMEM for 24 h, and then switched to media containing 10% FBS and 4-PBA (1 mmol/L) or 4μ8C (10 μmol/L) for 24 h for analysis of protein expression, immunofluorescence staining, EdU incorporation assay and cell cycle, or for 48 h for proliferation assay. DMSO served as a solvent control, and its final concentration was less than 0.1%.

2.16. Immunofluorescence staining in PASMCs

PASMCs were incubated with specific antibodies for XBP1s, Ki67, SERCA2, or calnexin (Cat# 66903-1-Ig; Proteintech) for 12 h, followed by Alexa Fluor 488 goat anti-rabbit IgG (H + L) or Cy3-conjugated Affinipure goat anti-mouse IgG (H + L) for 2 h. Stained nuclei with DAPI or Hoechst 33258 for 10 min. Monitored the fluorescence signals by microscopy (Leica DM6) and analyzed them by Las X software.

2.17. Construction of adenoviral expression vector for *ATP2A2a* (SERCA2a) S674

We constructed adenoviral expression vector of *ATP2A2a* S674 according to the previously published procedure[15]. Briefly, using pcDNA3.1-human *ATP2A2a* plasmid (Cat# 75187; Addgene, Watertown, MA, USA) as template, the full-length *ATP2A2a* S674 was obtained by point mutation using multiple PCR technology, and then cloned into pShuttle CMV vector (Cat# 16403; Addgene). The correct direction was confirmed by enzyme restriction analysis as well as sequencing. The adenovirus scaffold vector pAdEasy-1 (Shanghai Weidi Biotechnology Co., Ltd., China), containing most of the human adenovirus serotype 5 (Ad5) genome, is deleted for the genes E1 and E3. pshuttle-*ATP2A2a* S674 was linearized and then recombined with pAdEasy-1 in BJ5183 cells and colonies were screened for the appropriate constructs using restriction enzyme analysis. The appropriate cosmids were linearized with restriction enzyme and transfected into HEK293A cells for packaging and amplification.

2.18. Transfection of PASMCs

WT PASMCs were transfected with adenovirus *ATP2A2a* S674, *ATP2A2b* S674[15] or empty adenovirus; SKI PASMCs were transfected with adenovirus *ATP2A2b* C674 or empty adenovirus, with 50 multiplicity of infection (MOI)/cell in DMEM respectively without serum and antibiotics for 6 h before switching to DMEM containing 5% FBS for 48 h. Cells were collected for intracellular calcium measurement, Western blot, and proliferation assay. For *Xbp1s* plasmid[16] transfection, WT PASMCs were transfected with *Xbp1s* plasmid or its vector control (pcDNA3.1) using Effectene Transfection Reagent (Cat# 301425; Qiagen, Germantown, MD, USA) in DMEM for 48 h. Cells were collected for Western blot, XBP1 and Ki67 immunofluorescence staining, and proliferation assay.

2.19. Statistical analysis

For all data analysis, the outcome assessors were blind to the animal code. That is, one person assigned the animal code, while others did data analysis without knowing the animal code, and then regrouped data according to the animal code. Group size is the number of independent values, which used for statistical analysis. In some experiments, we used ratio to control to avoid the larger variation among different experiments. The mean values of the control group were normalized to 1. Except for the thrombosis result, other results were presented as mean ± standard error of mean (SEM). The incidence of PA thrombosis was analyzed by Chi-square test. Comparisons between experimental groups were performed with an unpaired *t*-test or by ANOVA for multiple comparisons with a Bonferroni correction or a Dunnett's multiple comparisons test. Values of $P < 0.05$ were considered statistically significant.

3. Results

3.1. Hypoxia increases the irreversible oxidation of SERCA2 C674 and decreases SERCA2 in lungs and PASMCs

Hypoxic PH is a commonly studied animal model of PH or PAH[2]. Hypoxia increases ROS generation and intracellular Ca^{2+} in PASMCs[17]. In the hypobaric-hypoxia induced PH mouse model[12], we used specific antibody targeting SERCA2 C674-SO_3H to detect the irreversible oxidation of C674[18]. Compared with normoxia, hypoxia increased the expression of C674-SO_3H in remodeled PAs (Supporting Information Fig. S1A). In lungs (Fig. S1B) and PASMCs (Fig. S1C) exposed to hypoxia, the

expression of C674-SO_3H increased, while total SERCA2 decreased, suggesting that they may be involved in PH.

3.2. *The substitution of C674 by S674 increases right ventricular pressure and induces pulmonary vascular remodeling*

Next, we used the heterozygous SKI without any induction to study the contribution of C674 oxidative inactivation to PH. Due to the difficulty to detect PAP in mouse, so we measured the right ventricular pressure to reflect PAP. RVSP of SKI increased with age, especially at 12 months old, while that of WT did not. RVEDP of SKI trended to increase compared with WT at all ages. Accordingly, right ventricular hypertrophy increased with age in SKI assessed by the Fulton Index, especially at 12 months old. The body weight showed no difference between SKI and WT at the same age (Fig. 1A).

As shown in Fig. 1B and Supporting Information Fig. S2, there were various types of pulmonary vascular remodeling, including PA remodeling (tunica media hypertrophy, the concentric or eccentric neointimal lesions, plexiform lesions, fibrosis, and thrombosis), and pulmonary vein remodeling (pulmonary venous hypertrophy) in SKI but not in WT, especially at 12 months old. Tunica media thickness of the resistance PAs (50- to 100-μm diameter) is an important early indicator of PA remodeling. It increased with age in SKI but not in WT. Cellular neointima in small PAs (around 50 μm diameter) occurred early as in 2-month old SKI, but the incidence decreased with age (Fig. 1B). Next, we analyzed and scored the severity of vascular remodeling based on various stages of pulmonary vascular lesions. Compared with WT of the same age, the neointimal lesions in SKI were more serious, especially at 4 months old. The stalk-like and aneurysm-like plexiform lesions became more severe in older SKI, especially at 12 months of age, while these lesions barely occurred in WT (Fig. 1B). In 12-month-old SKI, fibrosis broadly occurred in neointima, tunica media, and plexiform lesions of PAs (Fig. S2). Since SKI developed similar plexiform lesions to human PH, we scored lesions based on Heath-Edward classification that was later revised[14]. The grading increased with age in SKI but not in WT (Fig. 1B). In SKI, the average grade was between I and II (> 50% at grade II, reversible) at 2 months old, and grade III at both 4 months old (75% at grade III, critical) and 12 months old (> 60% at grade IV, irreversible). The incidence of thrombosis in PAs increased with age in SKI but not in WT (Fig. 1B). A substantial proportion of PH patients have pulmonary vein remodeling[19]. We found that most SKI at 2 months old had pulmonary venous hypertrophy. Compared with WT at the same age, the scores of venous lesions were higher in SKI at 4 and 12 months old (Fig. 1B). The muscularization of distal pulmonary arterioles (< 50-μm-diameter) is another important indicator of PA remodeling. Similar to literature[20], the percentage of non-muscularization is about 60%. There were higher percentages of partial and full muscularization of distal pulmonary arterioles in SKI than WT at the same age (Fig. 1C). Hyperproliferation is the cellular basis of vascular remodeling. The cell proliferation index Ki67-positive cells in SKI lung were more than those in WT lung. We particularly counted them in PA tunica media, which showed that the percentage of Ki67-positive cells in SKI was higher than that in WT, especially at 2 and 4 months old (Fig. 1D). As shown in Supporting Information Fig. S3, SMCs majorly contributed to SKI PA tunica medial hypertrophy, neointimal lesions, plexiform lesions, muscularization of distal pulmonary arterioles, and pulmonary venous hypertrophy, while ECs contributed to SKI cellular neointimal lesions and stalk-like plexiform lesions. All of these lesions were accompanied by Ki67-positive staining (Supporting Information Fig. S4), suggesting that C674 inactivation induced pulmonary vascular remodeling by promoting cell proliferation.

3.3. *The substitution of C674 by S674 promotes PASMC proliferation by accelerating cell cycle*

PASMC proliferation is an important cellular basis for pulmonary vascular remodeling. Therefore, we cultured primary PASMCs with α-SMA and SM22α positive immunostaining (Supporting Information Fig. S5A). In quiescent PASMCs, the main isoform of *Atp2a2* is *Atp2a2b*, whose relative copy number was at least 200 times that of *Atp2a2a* (Fig. 2A). The substitution of C674 had no effect on the mRNA and protein levels of SERCA2 (Fig. 2A) or its ER location (Fig. S5B). However, it increased the intracellular Ca^{2+} level (Fig. 2B) and the percentage of EdU-positive (Fig. 2C) or Ki67-positive proliferating cells (Supporting Information Fig. S6), and promoted PASMC proliferation (Fig. 2D). Compared with WT PASMCs, SKI PASMCs had more cells in S and G2/M phases and fewer cells in G0/G1 phase (Fig. 2E), which was consistent with the increase of protein expression of cell cycle related proteins, including A-type cyclins (A1 and A2), cyclin B1, CDK1 and CDK2, but had no effect on cyclin D1 (Fig. 2F). The increased expression of A-type cyclins and cyclin B1 in SKI PASMCs was further confirmed in the remodeled SKI pulmonary vessels (Fig. 2F).

3.4. *The substitution of C674 by S674 induces ER stress to promote PASMC proliferation*

SERCA is the only enzyme to take up intracellular Ca^{2+} into ER and maintain ER Ca^{2+} store which is imperative for ER normal function, in contrast, the sustained ER Ca^{2+} depletion causes ER stress[21,22]. ER stress is an important contributor to hypoxia- or monocrotaline-induced PH[23–25], which could be improved by its inhibitor 4-PBA[26,27]. In PASMCs, the substitution of C674 increased the expression of p-IRE1α, an active form of IRE1α, without affecting ER chaperone BIP and ER stress sensors of ATF6 and IRE1α (Fig. 3A). The active IRE1α has endoribonuclease activity to cleave *Xbp1u* mRNA to generate *Xbp1s* mRNA[22,28], whose corresponding proteins XBP1u and XBP1s are closely related to cell cycle and cell proliferation[16,29,30]. As shown in Fig. 3A, the substitution of C674 had no effect on XBP1u, but it increased XBP1s. In SKI PASMCs, 4-PBA inhibited the expression of p-IRE1α, XBP1s, and cell cycle related proteins, but not XBP1u (Fig. 3B). 4-PBA decreased the proportion of XBP1s and Ki67-positive cells (Fig. 3C), decreased the percentage of EdU-positive cells (Supporting Information Fig. S7), prevented cells from G0/G1 phase entering into S and G2/M phases (Fig. 3D), and inhibited cell proliferation (Fig. 3E), all of which indicated that the substitution of C674 by S674 promoted PASMC proliferation by inducing ER stress.

3.5. *Upregulation of XBP1s promotes SKI PASMC proliferation*

At mRNA level, the substitution of C674 had no effect on *Xbp1u*, but increased *Xbp1s* (Fig. 4A). XBP1s was highly expressed in SKI PASMCs (Fig. 4B) and pulmonary vessels (Fig. 4C). In WT PASMCs, overexpression of *Xbp1s* plasmid upregulated the expression of cell cycle related proteins (Fig. 4D), increased the percentage of Ki67-positive cells (Fig. 4E) and promoted cell proliferation (Fig. 4F).

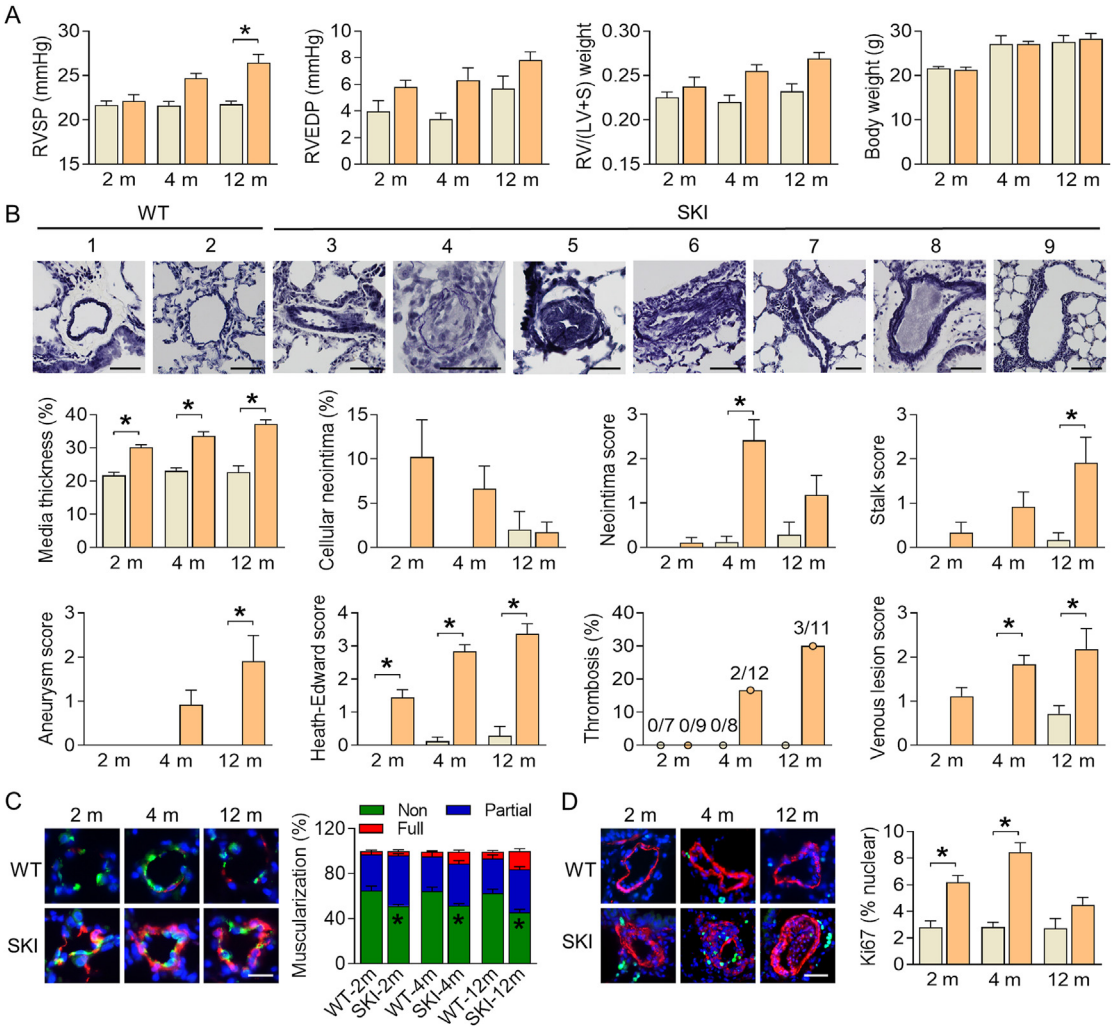

Figure 1 The substitution of C674 by S674 increases right ventricular pressure and induces pulmonary vascular remodeling. Cyan yellow bar indicates WT; orange bar indicates SKI [(A), (B), and (D)]. (A) Right ventricular systolic pressure (RVSP), right ventricular end-diastolic pressure (RVEDP), Fulton index, and body weight. RV, right ventricle; LV, left ventricle; S, interventricular septum. Fulton Index is the ratio of the weight of RV to the weight of LV plus S [RV/(LV + S) weight]. (B) Various types of pulmonary vascular remodeling indicated by Verhoeff-van Gieson staining and a summary of their severity in the graph. 1−2 from WT: 1, normal pulmonary artery (PA); 2, normal vein. 3−9 from SKI: 3, tunica media hypertrophy; 4, cellular neointima; 5, concentric neointimal lesion; 6, stalk-like plexiform lesion; 7, aneurysm-like plexiform lesion; 8, PA thrombosis; 9, venous hypertrophy. Scale bar: 50 μm. $^*P < 0.05$, SKI *vs.* WT at the same age, $n = 7$−12. (C) Muscularization of distal pulmonary arterioles indicated by α-smooth muscle actin (α-SMA) staining (red) and von Willebrand factor (vWF) staining (green). Scale bar: 25 μm. $^*P < 0.05$, the percentages of partially and fully muscularization in SKI *vs.* those in WT at the same age, $n = 6$−10. (D) The percentage of Ki67 (green) positive staining in PA tunica media indicated by α-SMA (red). Nuclei are indicated by DAPI (blue). Scale bar: 50 μm. $^*P < 0.05$, SKI *vs.* WT at the same age, $n = 7$−12. Data were presented as mean ± SEM except for the thrombosis result. The incidence of PA thrombosis is analyzed by Chi-square test. Others are analyzed by ANOVA with Bonferroni correction. m indicates month.

3.6. Inhibition of IRE1α/XBP1s pathway suppresses SKI PASMC proliferation

4μ8C, a substrate-specific inhibitor of IRE1α endoribonuclease, suppresses hypoxia-induced rat PASMC proliferation[31]. In SKI PASMCs, 4μ8C decreased the expression of XBP1s and the percentage of Ki67-positive cells (Fig. 5A) or EdU-positive cells (Fig. S7); 4μ8C downregulated cell cycle related proteins (Fig. 5B), prevented cells from G0/G1 phase entering into S and G2/M phases (Fig. 5C), and inhibited cell proliferation (Fig. 5D).

3.7. Inhibition of IRE1α/XBP1s pathway prevents SKI pulmonary vascular remodeling

Next, we gave the 4-week-old WT and SKI 4μ8C or solvent control (Ctrl) for 4 weeks to test if inhibition of the IRE1α/XBP1s pathway could prevent pulmonary vascular remodeling. The reason why we chose this age endpoint is because that the pulmonary vascular remodeling in SKI of this age was reversible. In the first round of *in vivo* studies, between WT/4μ8C and WT/Ctrl, there was no difference about body weight, right ventricular pressure, Fulton Index (Supporting Information Fig. S8A), pulmonary vascular remodeling

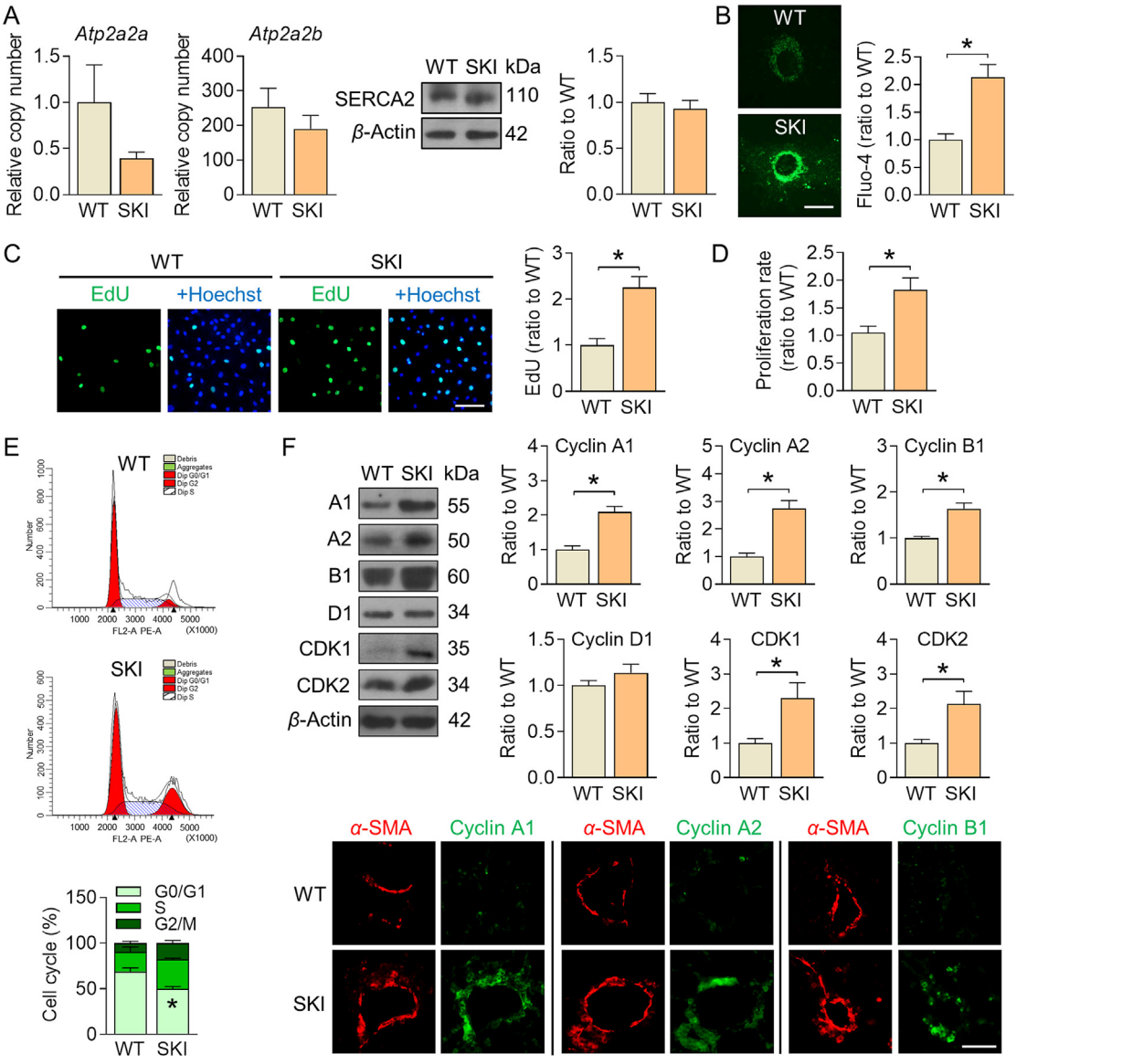

Figure 2 The substitution of SERCA2 C674 by S674 promotes PASMC proliferation by accelerating cell cycle. (A) The mRNA (left) and protein (right) levels of SERCA2 in PASMCs. mRNA, $n = 5$ (*Atp2a2a* are not detectable in two samples); protein, $n = 5$. (B) The intracellular Ca^{2+} level detected by Fluo-4 (green). Scale bar: 25 μm. (C) The percentage of EdU-positive proliferating cells (green). Nuclei are indicated by Hoechst 33258 (blue). Scale bar: 100 μm. (B) and (C), $^*P < 0.05$, SKI *vs.* WT, unpaired *t*-test, $n = 5$. (D) Cell proliferation. $^*P < 0.05$, SKI *vs.* WT, unpaired *t*-test, $n = 10$. (E) Representative cell cycle analyzed by flow cytometry and the relative percentage of cells in each phase. $^*P < 0.05$, G0/G1 phase or S phase, SKI *vs.* WT, ANOVA with Bonferroni correction, $n = 3$. (F) Cell cycle related proteins in PASMCs and in the remodeled SKI pulmonary vessels indicated by α-SMA staining (red). Scale bar: 50 μm. $^*P < 0.05$, SKI *vs.* WT, unpaired *t*-test, $n = 5–6$. Data were presented as mean ± SEM.

indexes (Fig. S8B), and the expression of XBP1 and cell cycle related proteins (Fig. S8C). Thus, we did not apply 4μ8C further in WT, and only compared three groups (WT/Ctrl, SKI/Ctrl, and SKI/4μ8C). Among these three groups, there were no differences in body weight, right ventricular pressure and Fulton Index (Supporting Information Fig. S9). The pulmonary vascular remodeling indexes (PA tunica media thickness, percentage of cellular neointima, Heath-Edward and venous lesion scores, percentage of non-muscularization or partial muscularization of distal pulmonary arterioles, and percentage of Ki67-positive cells in PA tunica media) in SKI were improved by 4μ8C to the levels comparable to WT (Fig. 6A). In SKI lungs, the increased XBP1s and cell cycle related proteins were reversed by 4μ8C (Fig. 6B). 4μ8C slightly increased XBP1u in SKI lungs, probably by suppressing the splicing of *Xbp1u*, thus causing its protein accumulation.

3.8. *SERCA2b inhibits IRE1α/XBP1s pathway and proliferation of SKI PASMCs*

In WT PASMCs, overexpression of *ATP2A2a* S674 or *ATP2A2b* S674 increased intracellular Ca^{2+} (Fig. 7A), promoted cell proliferation, upregulated the expression of p-IRE1α and XBP1s, without affecting

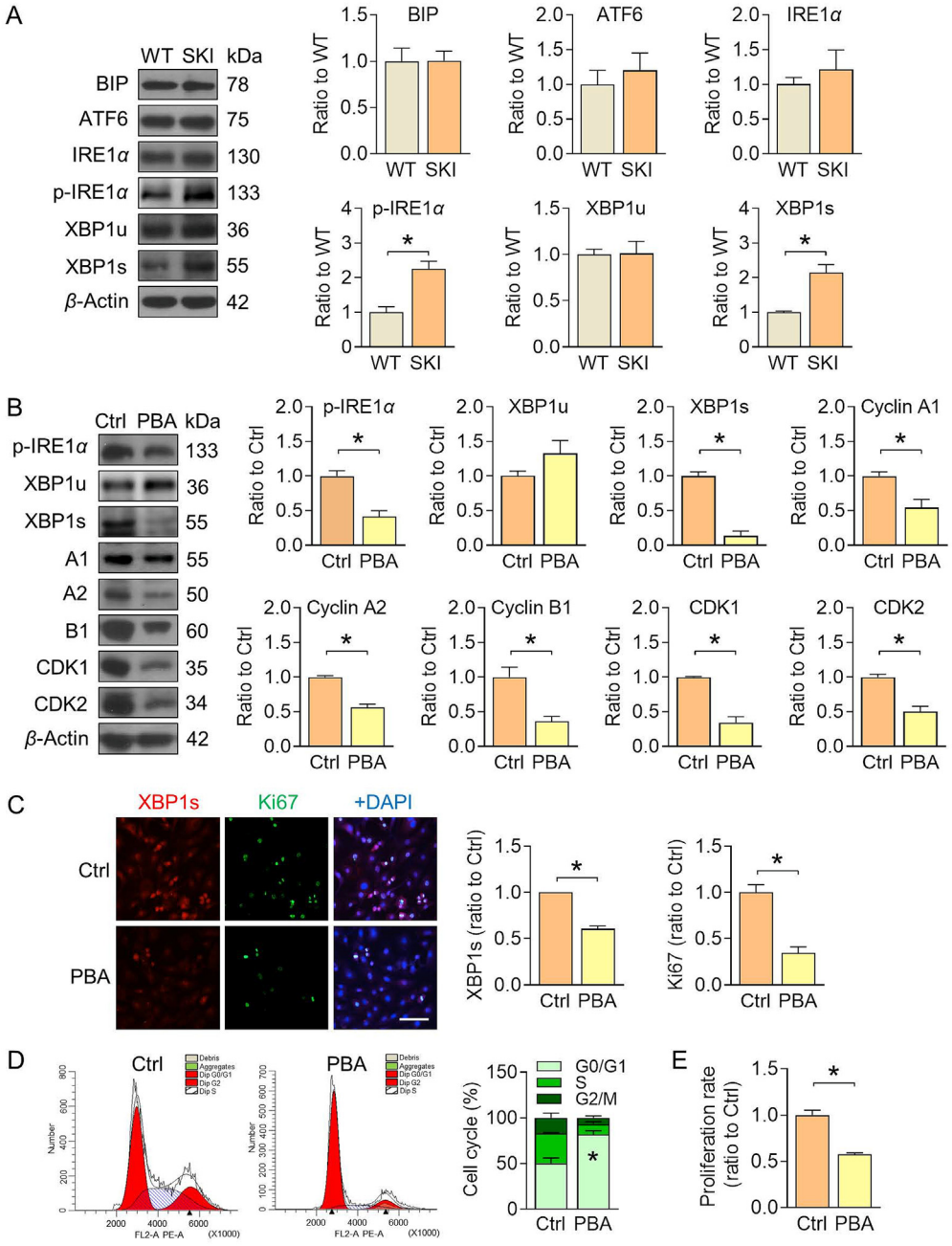

Figure 3 The substitution of SERCA2 C674 by S674 induces ER stress to promote PASMC proliferation. (A) Representative Western blot of ER stress related proteins in PASMCs and quantification of band intensities in graph. *$P < 0.05$, SKI *vs.* WT, unpaired *t*-test, $n = 5–6$. (B) Representative Western blot of SKI PASMCs treated with ER stress inhibitor 4-phenylbutyric acid (PBA), and quantification of band intensities in graph. *$P < 0.05$, PBA *vs.* solvent control (Ctrl), unpaired *t*-test, $n = 5–6$. (C) The expression of XBP1s (red) and the percentage of Ki67-positive (green) cells. Nuclei are indicated by DAPI (blue). *$P < 0.05$, PBA *vs.* Ctrl in SKI PASMCs, unpaired *t*-test, $n = 5$. (D) Representative cell cycle analyzed by flow cytometry (left), and the relative percentage of cells in each phase (right). *$P < 0.05$, all phases, PBA *vs.* Ctrl in SKI PASMCs, ANOVA with Bonferroni correction, $n = 3$. (E) Cell proliferation. *$P < 0.05$, PBA *vs.* Ctrl in SKI PASMCs, unpaired *t*-test, $n = 5$. Data were presented as mean ± SEM.

XBP1u (Fig. 7B). These confirmed that the substitution of C674 by S674 at either SERCA2a or SERCA2b could interfere with SERCA2 function, thus activated IRE1α/XBP1s pathway to promote PASMC proliferation. In SKI PASMCs, overexpression of *ATP2A2b* C674 inhibited cell proliferation and downregulated the expression of p-IRE1α, XBP1s, XBP1u, cyclin A1, cyclin A2, and cyclin D1 (Fig. 7C).

4. Discussion

SERCA2 is the major subtype of SERCA in pulmonary vasculature to maintain calcium homeostasis. The redox status of C674 in the SERCA2 is closely related to cardiovascular health and disease[21,32,33], but its role in pulmonary vascular remodeling and PH

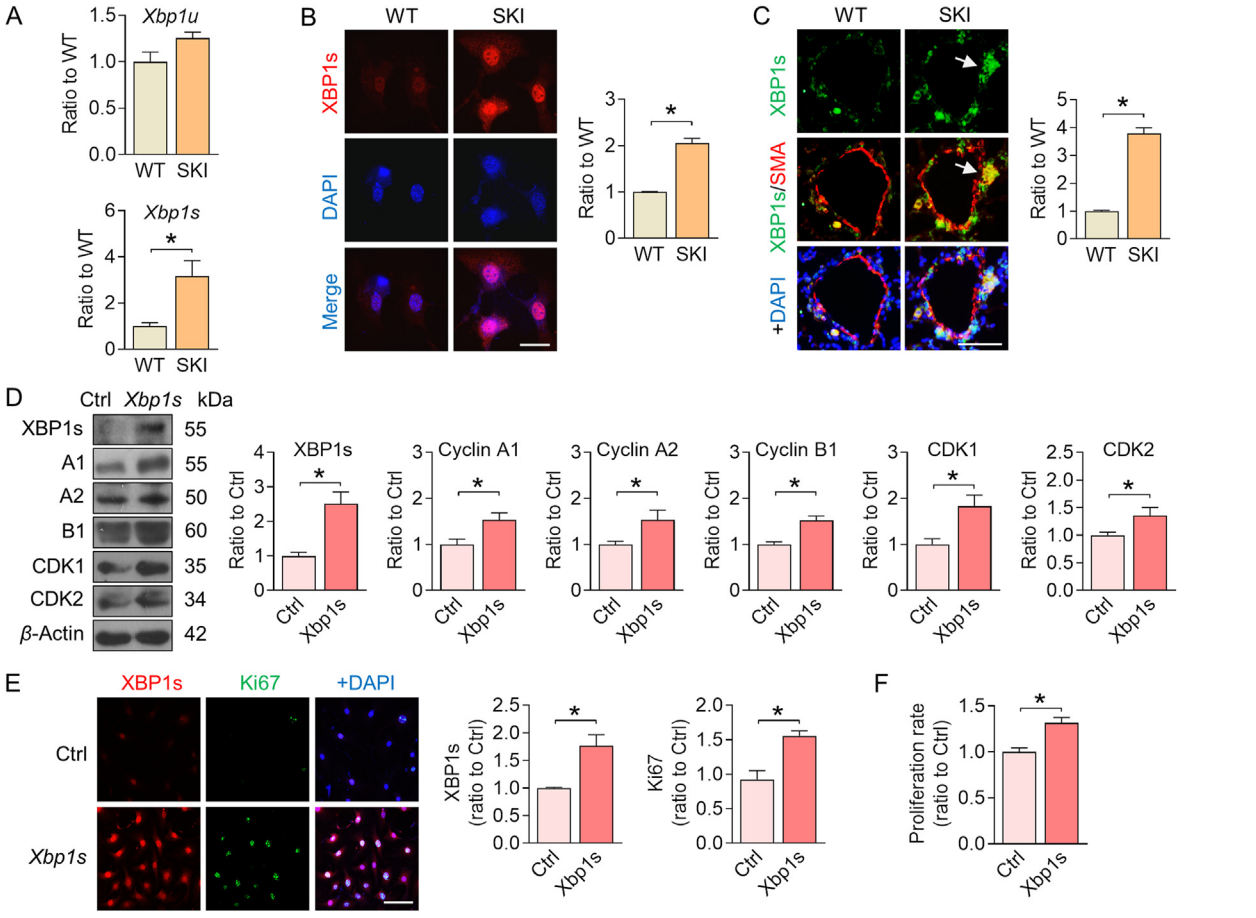

Figure 4 Upregulation of XBP1s promotes SKI PASMC proliferation. (A) *Xbp1* mRNA in PASMCs. $n = 5–9$. (B) Representative images of XBP1s immunofluorescence staining (red) in PASMCs and quantitative analysis of fluorescence density in graph. Nuclei are indicated by DAPI (blue). $n = 5$. Scale bar: 50 μm. (C) Representative images of XBP1s immunofluorescence staining (green) in pulmonary vessels indicated by α-SMA staining (red), and quantitative analysis of fluorescence density in graph. $n = 5$. The white arrow indicates that XBP1s is mainly expressed in the remodeled pulmonary vessels. Scale bar: 50 μm. (A)–(C), $^*P < 0.05$, SKI *vs.* WT, unpaired *t*-test. (D) Representative Western blot of WT PASMCs overexpressed *Xbp1s* plasmid or vector control (Ctrl), and quantification of band intensities in graph. $^*P < 0.05$, *Xbp1s vs.* Ctrl, unpaired *t*-test, $n = 3–7$. (E) The relative percentage of XBP1s (red) or Ki67-positive (green) cells in WT PASMCs overexpressed *Xbp1s* plasmid or vector control (Ctrl). $^*P < 0.05$, *Xbp1s vs.* Ctrl, unpaired *t*-test, $n = 5$. Scale bar: 100 μm. (F) Cell proliferation in WT PASMCs. $^*P < 0.05$, *Xbp1s vs.* Ctrl, unpaired *t*-test, $n = 5$. Data were presented as mean ± SEM.

remains unclear. C674 is the key cysteine and can be glutathiolated by nitric oxide to increase SERCA2 activity in aortic SMCs, and when C674 is irreversibly oxidized by high levels of ROS or replaced by S674, the nitric oxide-induced SERCA2 activity is blocked[7,33]. Here we use hypoxia-induced PH mouse model, characterized by increased ROS generation in PASMCs[17], to address the potential link of the irreversible oxidation of SERCA2 C674 to pulmonary vascular remodeling. In hypoxic remodeled PAs, C674-SO_3H is significantly increased. We speculate that the irreversible oxidative inactivation of C674 may promote pulmonary vascular remodeling and PH. Using SKI to mimic C674 oxidative inactivation, we find that the substitution of C674 by S674 without affecting the total SERCA2 expression, significantly promotes baseline PASMC proliferation in the absence of nitric oxide donor, causes pulmonary vascular remodeling, and modestly increases RVSP with age. This demonstrates the causal effect of C674 inactivation on the development of pulmonary vascular remodeling and PH, and emphasizes the importance of C674 redox state in controlling PASMC functions and pulmonary vascular homeostasis. In PASMCs, the substitution of C674 by S674 induces ER stress, specifically the activation of IRE1α/XBP1s pathway, upregulates the expression of cell cycle related proteins and accelerates cell cycle. These effects culminate in promoting cell proliferation and pulmonary vascular remodeling, ultimately increasing pulmonary vascular resistance. Early inhibition of the IRE1α/XBP1s pathway prevents pulmonary vascular remodeling caused by the substitution of C674. Similar to SERCA2a[9], SERCA2b is also important to restrict the proliferation of PASMCs. We hypothesize that in pathological conditions (such as obesity, insulin resistance, diabetes, hypoxia, aging, virus infection, inflammation, and many other diseases that persistently produce a large amount of ROS in lungs) the oxidative inactivation of SERCA2 C674 and the activation of downstream IRE1α/XBP1s pathway may be one of the common mechanisms of various PH.

SKI spontaneously develop pulmonary vascular lesions, showing common features of human PH, such as vessel medial hypertrophy, muscularization and lumen obliteration of the small

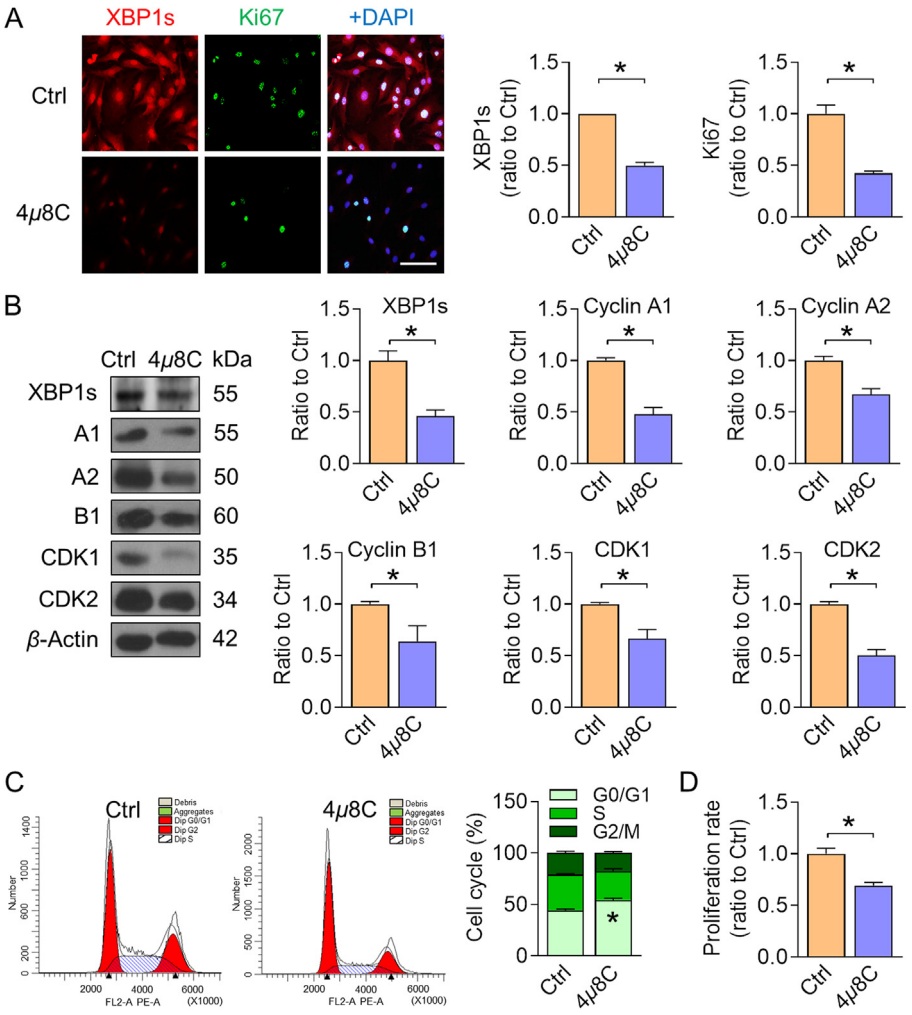

Figure 5 Inhibition of the IRE1α/XBP1s pathway suppresses SKI PASMC proliferation. (A) Representative images of XBP1s (red) and Ki67 (green) immunofluorescence staining in SKI PASMCs treated with 4μ8C, and quantitative analysis of fluorescence density in graph. Nuclei are indicated by DAPI (blue). *$P < 0.05$, 4μ8C *vs.* solvent control (Ctrl), unpaired *t*-test, $n = 5$. Scale bar: 100 μm. (B) Representative Western blot of SKI PASMCs treated with 4μ8C, and quantification of band intensities in graph. *$P < 0.05$, 4μ8C *vs.* Ctrl, unpaired *t*-test, $n = 5$–6. (C) Representative cell cycle analyzed by flow cytometry in SKI PASMCs treated with 4μ8C, and the relative percentage of cells in each phase. *$P < 0.05$, G0/G1 phase or S phase, 4μ8C *vs.* Ctrl, ANOVA with Bonferroni correction, $n = 3$. (D) Cell proliferation. *$P < 0.05$, 4μ8C *vs.* Ctrl in SKI PASMCs, unpaired *t*-test, $n = 5$. Data were presented as mean ± SEM.

PAs. SKI develop complex plexiform lesions at 4- and 12- months of age with incidence 40%–50%, histologically resembling PAH patients[6]. It takes SKI up to 12 months to develop mild elevated right ventricular pressure and hypertrophy, similar to human idiopathic PAH (IPAH) that generally develops at elder age or is accompanied with ROS generating diseases[34–36]. The IPAH is the most common PAH that takes longer time to develop[35]. A large population of PH patients have obesity and diabetes, whose incidence in IPAH is significantly higher than other types of PAH[34–36]. High-fat diet induces mouse PH or exacerbates rat hypoxic PH[37,38], indicating that these ROS generating diseases promote the development of PH. As data not shown, we found that high-fat diet significantly increased C674-SO_3H in mouse lungs. Similar to SKI PASMCs, the expression of cyclin A2, CDK1, and CDK2 in IPAH PASMCs is upregulated, while the expression of D-type cyclins has no change[39], suggesting that SKI and IPAH may have similar pathogenesis.

SERCA2a is downregulated in pulmonary vessels of PAH patients, while its gene transfer decreases cyclin D1 in rat PASMCs and improves monocrotaline-induced rat pulmonary vascular remodeling[9]. There is no report about the effects of SERCA2 dysfunction on other cell cycle-related proteins and cell cycle. The substitution of C674 by S674 increases the expression of A-type cyclins, cyclin B1, CDK1, and CDK2, without affecting cyclin D1, accelerates cells entering into S and G2/M phases. Overexpression of *ATP2A2a* S674 or *ATP2A2b* S674 in WT PASMCs promotes cell proliferation and activates IRE1α/XBP1s pathway, without affecting XBP1u. The expression of XBP1u and cyclin D1 has no change in SKI, suggesting their limited contribution to hyperproliferation of SKI PASMCs. Because the mRNA level of SERCA2a is hardly detectable in cultured PASMCs, the substitution of C674 by S674 in SERCA2b might be the main factor to promote cell cycle and cell proliferation of SKI PASMCs. The overexpression of *ATP2A2b* C674 not only inhibits IRE1α/XBP1s

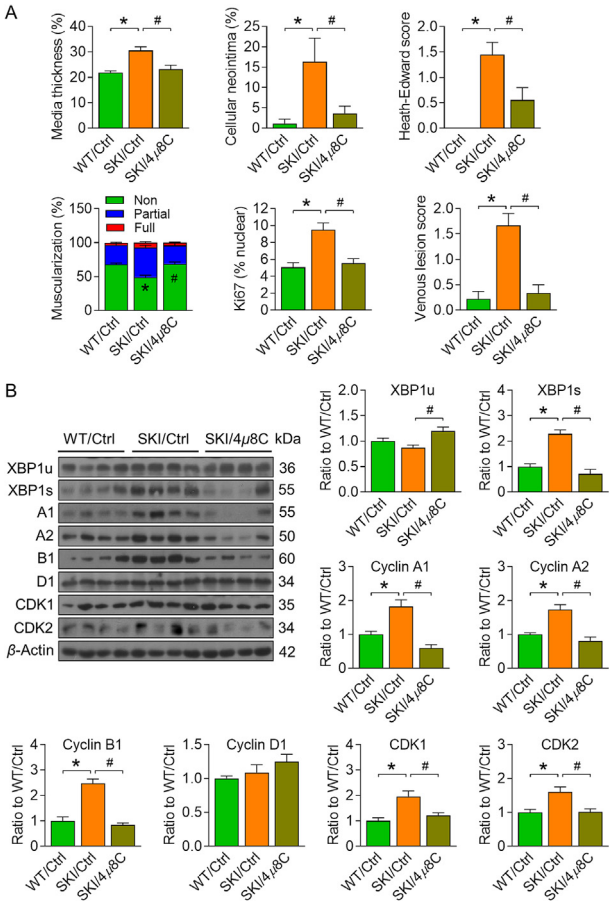

Figure 6 Inhibition of IRE1α/XBP1s pathway prevents SKI pulmonary vascular remodeling. (A) Summary of the severity of vascular remodeling in PAs and veins. (B) The protein expression of XBP1 and cell cycle related proteins in lungs. $^{*}P < 0.05$, SKI treated with solvent control (SKI/Ctrl) *vs.* WT treated with solvent control (WT/Ctrl), $^{\#}P < 0.05$, SKI treated with 4μ8C (SKI/4μ8C) *vs.* SKI/Ctrl. ANOVA with Bonferroni correction, $n = 9$. The WT/Ctrl group ($n = 9$) includes the data from Fig. S8 ($n = 5$). Data were presented as mean ± SEM.

pathway, A-type cyclins and cyclin B1, but also downregulates XBP1u and cyclin D1, and inhibits the proliferation of SKI PASMCs, suggesting its important roles in maintaining pulmonary vascular homeostasis. Its dysfunction also contributes to pulmonary vascular remodeling and PH. Similar to SERCA2a[9], selective pulmonary SERCA2b gene transfer might also improve pulmonary vascular remodeling. Gingerol, a natural product, is used as food supplement for functional dyspepsia[40]. It is a non-specific SERCA2 activator[41]. Whether gingerol or other SERCA2 activators can improve pulmonary vascular remodeling deserves further study. Overexpression of SERCA2a in PASMCs suppresses cell proliferation by inhibiting nuclear factor of activated T cells (NFAT) and signal transducer and activator of transcription-3 pathway[9]. As data not shown, the activation of NFAT pathway is also the cause of hyperproliferation of SKI PASMCs, and its detail mechanism is under investigation. However, we found that NFAT pathway and IRE1α/XBP1s pathway seemed to work independently in controlling SKI PASMC hyperproliferation.

Activation of XBP1s accelerates SMCs proliferation, leading to neointimal formation in femoral artery injury models[42]. However, its contribution in PASMCs is still unknown. Here we demonstrate the direct regulation of XBP1s in PASMCs on cell cycle related proteins and cell proliferation, and provide the evidence that the upregulated XBP1s is responsible for hyperproliferation of SKI PASMCs. 4μ8C by decreasing the expression of XBP1s, downregulates cell cycle related proteins, inhibits cell cycle and cell proliferation in SKI PASMCs, and prevents SKI pulmonary vascular remodeling. This is the first study that reports the activation of XBP1s promoting PASMC proliferation and pulmonary vascular remodeling by upregulating these cell cycle related proteins to accelerate cell cycle. Although 4μ8C had no effect on WT, it does improve pulmonary vascular remodeling when IRE1α/XBP1s pathway is activated. This is also the first report that confirms the inhibition of IRE1α/XBP1s pathway *in vivo* by 4μ8C improves pulmonary vascular remodeling. The reverse effect of 4μ8C on pulmonary vascular remodeling in SKI mice of different ages needs to be further studied. Tauroursodeoxycholic acid (TUDCA), an endogenous amphiphilic bile acid, is an effective ER stress inhibitor. TUDCA inhibits *Xbp1s* mRNA expression in intermittent hypoxia-induced pulmonary tissues[43] and improves pulmonary vascular remodeling[23]. Toyocamycin is a nucleoside-type antibiotic analogue of adenosine in clinic and an inhibitor of XBP1 activation induced by ER stress[44]. TUDCA and toyocamycin might improve SKI pulmonary vascular remodeling, which worth further exploration and study.

The reason why we construct whole-body SKI is because that in the pathological models of ROS increase, C674 is significantly irreversibly oxidized in various tissues[32,45–47], which means that C674 is widely inactivated by oxidation in the whole body. The homozygous SKI are embryo lethal, emphasizing the importance of C674[10]. In these SKI, angiogenesis is impaired after hindlimb ischemia, angiotensin II-induced aortic aneurysm worsened, and blood pressure increased by 10−20 mmHg[10,32,47]. PH is a complex disease, which is considered as the pulmonary manifestation of systemic diseases. Even in the lungs, bronchus interacts with pulmonary vessels to promote pulmonary vascular remodeling[6,48]. Besides PASMCs, ECs, fibroblasts, and inflammatory cells all contribute to pulmonary vascular remodeling[2]. We found that at least ECs and venous SMCs were involved in SKI pulmonary vascular remodeling. The activation of IRE1α/XBP1s pathway seems to be the common pathway since its inhibition improves cellular neointima derived from ECs and venous hypertrophy derived from SMCs. Although C674 is widely oxidized in various cells, the results may be different. In comparison with the sole activation of IRE1α/XBP1s pathway by substitution of C674 in PASMCs, it upregulated BIP, ATF6, p-PERK and C/EBP homologous protein (CHOP) in renal proximal tubule cells[47], aortic SMCs, coronary artery ECs, and macrophages from our unpublished data. Ca^{2+} triggers different signaling pathways depending on its concentration in a temporal and spatial manner, and might mainly depend on its local increase rather the overall increase, making its regulation more complex. The different expression levels and compositions of SERCA2 may explain the different fate of C674 inactivation in different cells and tissues. This SKI model provides a valuable tool not only for studying the individual contribution of different cell types and tissues, but also for studying the contribution of their interaction to pulmonary vascular remodeling.

5. Conclusions

Our data provide direct evidence that C674 in SERCA2, especially in SERCA2b, restricts PASMC proliferation by

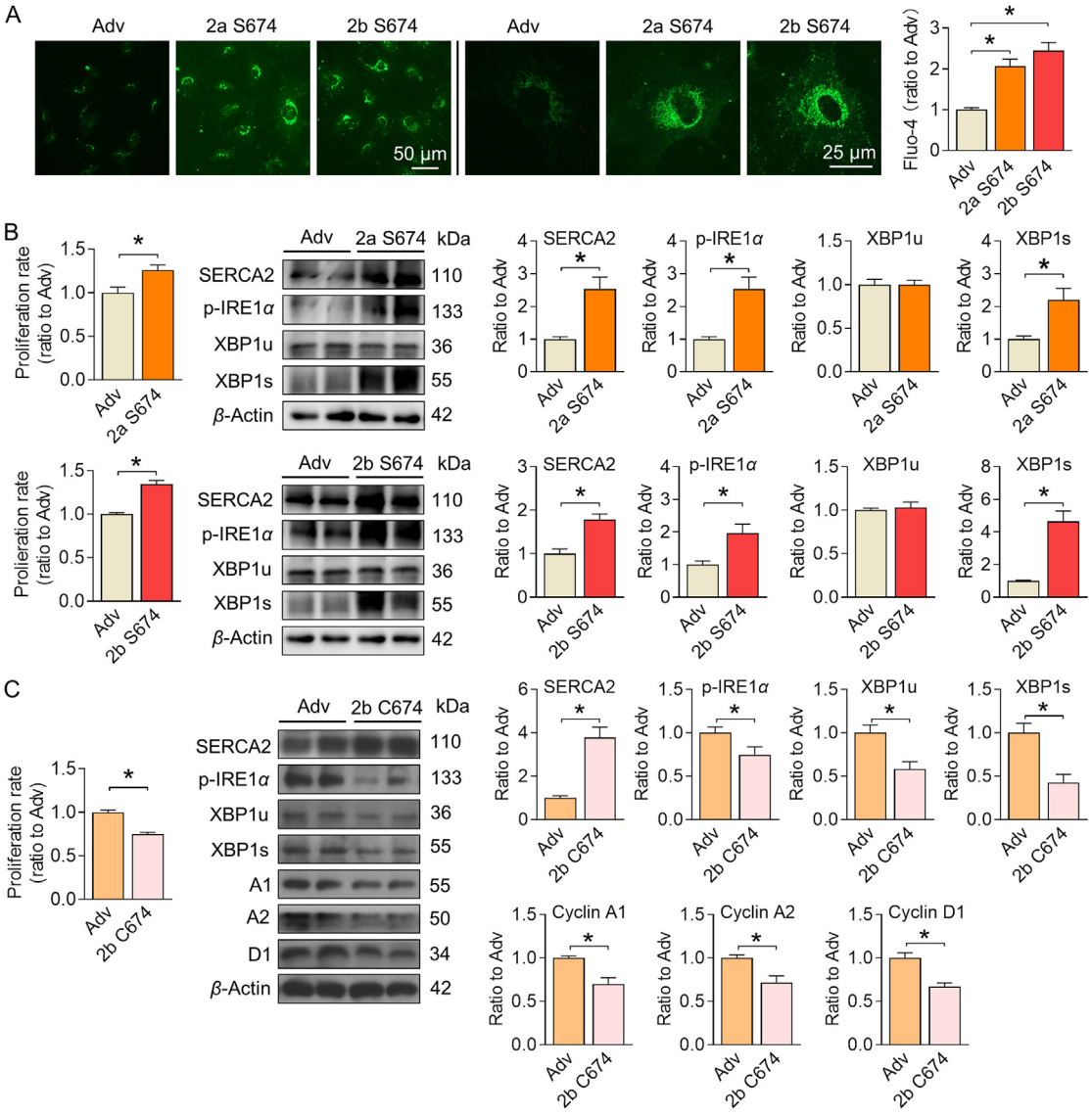

Figure 7 SERCA2b inhibits IRE1α/XBP1s pathway and proliferation of SKI PASMCs. (A) Overexpression of adenovirus *ATP2A2a* S674 or *ATP2A2b* S674 increased intracellular Ca^{2+} in WT PASMCs. *$P < 0.05$, *ATP2A2a* S674 or *ATP2A2b* S674 *vs.* empty adenovirus control (Ctrl), ANOVA with Bonferroni correction, $n = 5$. (B) Overexpression of adenovirus *ATP2A2a S674* or *ATP2A2b* S674 on cell proliferation and protein expression of p-IRE1α and XBP1s in WT PASMCs. *$P < 0.05$, *ATP2A2a* S674 or *ATP2A2b* S674 *vs.* Ctrl, unpaired *t*-test, $n = 5–6$. (C) Overexpression of adenovirus *ATP2A2b* C674 on cell proliferation and protein expression of p-IRE1α, XBP1s and cell cycle related proteins in SKI PASMCs. *$P < 0.05$, *ATP2A2b* C674 *vs.* Ctrl, unpaired *t*-test, $n = 4–9$.

suppressing the activation of IRE1α/XBP1s pathway, thus maintaining pulmonary vascular homeostasis. SKI develop pulmonary vascular remodeling which histologically resembles PH patients, and might become a valuable tool for the etiological research and drug screening of pulmonary vascular remodeling and PH. The oxidative inactivation of SERCA2 C674 and its downstream activation of the IRE1α/XBP1s pathway might be one of the common mechanisms of various PH. The IRE1α/XBP1s pathway and SERCA2 might be potential targets for PH therapy.

Acknowledgments

This study was supported by National Natural Science Foundation of China (31571172 and 81870343 to Xiaoyong Tong, 81700237 to Pingping Hu); Chongqing Natural Science Foundation (cstc2021jcyj-msxmX0043 to Xiaoyong Tong, China); Chongqing Research Program of Basic Research and Frontier Technology (cstc2016jcyjA0407 to Xiaoyong Tong, China); Fundamental Research Funds for the Central Universities (2018CDQYYX0042 to Xiaoyong Tong, and 2018CDYXYX0027 to Pingping Hu, China).

Author contributions

Weimin Yu and Xiaoyong Tong conceptualized the experiments for this manuscript. Weimin Yu, Gang Xu, Hui Chen, Li Xiao, Gang Liu, and Pingping Hu performed experiments and analysis. Vivi Kasim provided the resources. Weimin Yu, Siqi Li, and Xiaoyong Tong wrote the original draft of the manuscript. Chunyu Zeng provided intelligent input.

Conflicts of interest

Weimin Yu, Li Xiao, Hui Chen, Pingping Hu, and Xiaoyong Tong have used some data in this paper to apply for a Chinese patent.

Appendix A. Supporting information

Supporting data to this article can be found online at https://doi.org/10.1016/j.apsb.2021.12.025.

References

1. Simonneau G, Gatzoulis MA, Adatia I, Celermajer D, Denton C, Ghofrani A, et al. Updated clinical classification of pulmonary hypertension. *J Am Coll Cardiol* 2013;**54**:S43–54.
2. Stenmark KR, Meyrick B, Galie N, Mooi WJ, McMurtry IF. Animal models of pulmonary arterial hypertension: the hope for etiological discovery and pharmacological cure. *Am J Physiol Lung Cell Mol Physiol* 2009;**297**:L1013–32.
3. Simonneau G, Montani D, Celermajer DS, Denton CP, Gatzoulis MA, Krowka M, et al. Haemodynamic definitions and updated clinical classification of pulmonary hypertension. *Eur Respir J* 2019;**53**:1801913.
4. Ghigna MR, Dorfmüller P. Pulmonary vascular disease and pulmonary hypertension. *Diagn Histopathol* 2019;**25**:304–12.
5. Michael E, Yeager KLC. Animal models of pulmonary hypertension: matching disease mechanisms to etiology of the human disease. *J Pulm Respir Med* 2014;**4**:198.
6. Humbert M, Guignabert C, Bonnet S, Dorfmüller P, Klinger JR, Nicolls MR, et al. Pathology and pathobiology of pulmonary hypertension: state of the art and research perspectives. *Eur Respir J* 2019;**53**:1801887.
7. Adachi T, Weisbrod RM, Pimentel DR, Ying J, Sharov VS, Schöneich C, et al. *S*-Glutathiolation by peroxynitrite activates SERCA during arterial relaxation by nitric oxide. *Nat Med* 2004;**10**:1200–7.
8. Liu B, Wang D, Luo E, Hou J, Qiao Y, Yan G, et al. Role of TG2-mediated SERCA2 serotonylation on hypoxic pulmonary vein remodeling. *Front Pharmacol* 2020;**10**:1611.
9. Hadri L, Kratlian RG, Benard L, Maron BA, Dorfmüller P, Ladage D, et al. Therapeutic efficacy of AAV1.SERCA2a in monocrotaline-induced pulmonary arterial hypertension. *Circulation* 2013;**128**:512–23.
10. Thompson MD, Mei Y, Weisbrod RM, Silver M, Shukla PC, Bolotina VM, et al. Glutathione adducts on sarcoplasmic/endoplasmic reticulum Ca^{2+} ATPase Cys-674 regulate endothelial cell calcium stores and angiogenic function as well as promote ischemic blood flow recovery. *J Biol Chem* 2014;**289**:19907–16.
11. Que Y, Shu X, Wang L, Wang S, Li S, Hu P, et al. Inactivation of SERCA2 Cys674 accelerates aortic aneurysms by suppressing PPARγ. *Br J Pharmacol* 2021;**178**:2305–23.
12. Luo Y, Zhang B, Dong HY, Liu Y, Li ZC, Dong MQ, et al. Prevention of hypoxic pulmonary hypertension by hypoxia-inducible expression of p27 in pulmonary artery smooth muscle cells. *Gene Ther* 2014;**21**:751–8.
13. Cross BCS, Bond PJ, Sadowski PG, Jha BK, Zak J, Goodman JM, et al. The molecular basis for selective inhibition of unconventional mRNA splicing by an IRE1-binding small molecule. *Proc Natl Acad Sci U S A* 2012;**109**:E869–78.
14. Wagenvoort CA, Nauta J, van der Schaar PJ, Weeda HW, Wagenvoort N. The pulmonary vasculature in complete transposition of the greatvessels, judged from lung biopsies. *Circulation* 1968;**38**:746–54.
15. Ying J, Tong X, Pimentel DR, Weisbrod RM, Trucillo MP, Adachi T, et al. Cysteine-674 of the sarco/endoplasmic reticulum calcium ATPase is required for the inhibition of cell migration by nitric oxide. *Arterioscler Thromb Vasc Biol* 2007;**27**:783–90.
16. Huang C, Wu S, Ji H, Yan X, Xie Y, Murai S, et al. Identification of XBP1-u as a novel regulator of the MDM2/p53 axis using an shRNA library. *Sci Adv* 2017;**3**:e1701383.
17. Rathore R, Zheng YM, Niu CF, Liu QH, Korde A, Ho YS, et al. Hypoxia activates NADPH oxidase to increase [ROS]i and $[Ca^{2+}]$i through the mitochondrial ROS-PKCepsilon signaling axis in pulmonary artery smooth muscle cells. *Free Radic Biol Med* 2008;**45**:1223–31.
18. Cohen RA, Tong X. Vascular oxidative stress: the common link in hypertensive and diabetic vascular disease. *J Cardiovasc Pharmacol* 2010;**55**:308–16.
19. Ghigna MR, Guignabert C, Montani D, Girerd B, Jaïs X, Savale L, et al. BMPR2 mutation status influences bronchial vascular changes in pulmonary arterial hypertension. *Eur Respir J* 2016;**48**:1668–81.
20. Dromparis P, Paulin R, Sutendra G, Qi AC, Bonnet S, Michelakis ED. Uncoupling protein 2 deficiency mimics the effects of hypoxia and endoplasmic reticulum stress on mitochondria and triggers pseudo-hypoxic pulmonary vascular remodeling and pulmonary hypertension. *Circ Res* 2013;**113**:126–36.
21. Chemaly ER, Troncone L, Lebeche D. SERCA control of cell death and survival. *Cell Calcium* 2018;**69**:46–61.
22. D Thompson M. Endoplasmic reticulum stress and related pathological processes. *J Diagn Tech Biomed Anal* 2013;**1**:1000107.
23. Dromparis P, Paulin R, Stenson TH, Haromy A, Sutendra G, Michelakis ED. Attenuating endoplasmic reticulum stress as a novel therapeutic strategy in pulmonary hypertension. *Circulation* 2013;**127**:115–25.
24. Hu Y, Yang W, Xie L, Liu T, Liu H, Liu B. Endoplasmic reticulum stress and pulmonary hypertension. *Pulm Circ* 2020;**10**:2045894019900121.
25. Sutendra G, Dromparis P, Wright P, Bonnet S, Haromy A, Hao Z, et al. The role of nogo and the mitochondria-endoplasmic reticulum unit in pulmonary hypertension. *Sci Transl Med* 2011;**3**:88ra55.
26. Koyama M, Furuhashi M, Ishimura S, Mita T, Fuseya T, Okazaki Y, et al. Reduction of endoplasmic reticulum stress by 4-phenylbutyric acid prevents the development of hypoxia-induced pulmonary arterial hypertension. *Am J Physiol Heart Circ Physiol* 2014;**306**:H1314–23.
27. Zeng M, Sang W, Chen S, Liu Y, Zhang H, Kong X. Inhibition of ER stress by 4-PBA protects MCT-induced pulmonary arterial hypertension *via* reducing NLRP3 inflammasome activation. *Int J Clin Exp Pathol* 2017;**10**:4162–72.
28. Lin JH, Li H, Yasumura D, Cohen HR, Zhang C, Panning B, et al. IRE1 signaling affects cell fate during the unfolded protein response. *Science* 2007;**318**:944–9.
29. Thorpe JA, Schwarze SR. IRE1α controls cyclin A1 expression and promotes cell proliferation through XBP-1. *Cell Stress Chaperones* 2010;**15**:497–508.
30. Wang N, Zhao F, Lin P, Zhang G, Tang K, Wang A, et al. Knockdown of *XBP1* by RNAi in mouse granulosa cells promotes apoptosis, inhibits cell cycle, and decreases estradiol synthesis. *Int J Mol Sci* 2017;**18**:1152.
31. Cao X, He Y, Li X, Xu Y, Liu X. The IRE1α-XBP1 pathway function in hypoxia-induced pulmonary vascular remodeling, is upregulated by quercetin, inhibits apoptosis and partially reverses the effect of quercetin in PASMCs. *Am J Transl Res* 2019;**11**:641–54.
32. Que Y, Shu X, Wang L, Hu P, Wang S, Xiong R, et al. Inactivation of cysteine 674 in the SERCA2 accelerates experimental aortic aneurysm. *J Mol Cell Cardiol* 2020;**139**:213–24.
33. Tong X, Hou X, Jourd'Heuil D, Weisbrod RM, Cohen RA. Upregulation of Nox4 by TGFβ1 oxidizes SERCA and inhibits NO in arterial smooth muscle of the prediabetic zucker rat. *Circ Res* 2010;**107**:975–83.
34. Friedman SE, Andrus BW. Obesity and pulmonary hypertension: a review of pathophysiologic mechanisms. *J Obes* 2012;**2012**:505274.
35. Kopeć G, Kurzyna M, Mroczek E, Chrzanowski Ł, Mularek-Kubzdela T, Skoczylas I, et al. Characterization of patients with pulmonary arterial hypertension: data from the Polish registry of pulmonary hypertension (BNP-PL). *J Clin Med* 2020;**9**:173.
36. Taraseviciute A, Voelkel NF. Severe pulmonary hypertension in postmenopausal obese women. *Eur J Med Res* 2006;**11**:198–202.
37. Irwin DC, Garat CV, Crossno JT, Maclean PS, Sullivan TM, Erickson PF, et al. Obesity-related pulmonary arterial hypertension in

rats correlates with increased circulating inflammatory cytokines and lipids and with oxidant damage in the arterial wall but not with hypoxia. *Pulm Circ* 2014;**4**:638−53.
38. Kelley EE, Baust J, Bonacci G, Golin-Bisello F, Devlin JE, St Croix CM, et al. Fatty acid nitroalkenes ameliorate glucose intolerance and pulmonary hypertension in high-fat diet-induced obesity. *Cardiovasc Res* 2014;**101**:352−63.
39. Weiss A, Neubauer MC, Yerabolu D, Kojonazarov B, Schlueter BC, Neubert L, et al. Targeting cyclin-dependent kinases for the treatment of pulmonary arterial hypertension. *Nat Commun* 2019;**10**:2204.
40. Tursi A, Picchio M, Elisei W, Allegretta L, Benedicenti P, Bossa F, et al. Effectiveness and safety of a nutraceutical formulation for the treatment of functional dyspepsia in primary care. *Rev Recent Clin Trials* 2021;**16**:329−34.
41. Namekata I, Hamaguchi S, Wakasugi Y, Ohhara M, Hirota YTH. Ellagic acid and gingerol, activators of the sarco-endoplasmic reticulum Ca^{2+}-ATPase, ameliorate diabetes mellitus-induced diastolic dysfunction in isolated murine ventricular myocardia. *Eur J Pharmacol* 2013;**706**:48−55.
42. Zeng L, Li Y, Yang J, Wang G, Margariti A, Xiao Q, et al. XBP 1-deficiency abrogates neointimal lesion of injured vessels *via* cross talk with the PDGF signaling. *Arterioscler Thromb Vasc Biol* 2015;**35**:2134−44.
43. Shi Z, Xu L, Xie H, Ouyang R, Ke Y, Zhou R, et al. Attenuation of intermittent hypoxia-induced apoptosis and fibrosis in pulmonary tissues *via* suppression of ER stress activation. *BMC Pulm Med* 2020;**20**:92.
44. Ri M, Tashiro E, Oikawa D, Shinjo S, Tokuda M, Yokouchi Y, et al. Identification of toyocamycin, an agent cytotoxic for multiple myeloma cells, as a potent inhibitor of ER stress-induced *XBP1* mRNA splicing. *Blood Cancer J* 2012;**2**:e79.
45. Ying J, Sharov V, Xu S, Jiang B, Gerrity R, Schöneich C, et al. Cysteine-674 oxidation and degradation of sarcoplasmic reticulum Ca^{2+} ATPase in diabetic pig aorta. *Free Radic Biol Med* 2008;**45**:756−62.
46. Lancel S, Zhang J, Evangelista A, Trucillo MP, Tong X, Siwik DA, et al. Nitroxyl activates SERCA in cardiac myocytes *via* glutathiolation of cysteine 674. *Circ Res* 2009;**104**:720−3.
47. Liu G, Wu F, Jiang X, Que Y, Qin Z, Hu P, et al. Inactivation of Cys674 in SERCA2 increases BP by inducing endoplasmic reticulum stress and soluble epoxide hydrolase. *Br J Pharmacol* 2020;**177**:1793−805.
48. Mitzner W, Wagner EM. Vascular remodeling in the circulations of the lung. *J Appl Physiol* 2004;**97**:1999−2004.